Advances in Redox Research 19 (2026) 100168

Contents lists available at ScienceDirect

Advances in Redox Research

journal homepage: www.elsevier.com/locate/arres

Full Length Article

Intracellular copper redox modulation disrupts ROS–Ca^{2+} amplification in an ATP7B-deficient zebrafish model of Wilson's disease

Itzchak Angel [a,*], Kalaichitra Periyasamy [b], Micha Gladnikoff [c], Benin Joseph [b], Raphael Mayer [c], Erez Aminov [a]

[a] Telomir Pharmaceuticals Inc., Miami, FL, USA
[b] Pentagrit Discovery Lab, Chennai, Tamil Nadu, India
[c] Smart Assays Biotechnologies Ltd., Nes Ziona, Israel

ARTICLE INFO

Keywords:
Copper
Wilson's disease
ROS generation
Zebrafish
ATP7B mutants
Mitochondria

ABSTRACT

Excess labile copper catalyzes Fenton-type redox cycling, amplifying reactive oxygen species (ROS) and disrupting mitochondrial and calcium homeostasis. In Wilson's disease (WD), ATP7B deficiency leads to hepatic copper accumulation and progressive redox-driven tissue injury. Here, we investigated whether intracellular copper modulation interrupts ROS–Ca^{2+} amplification cascades and restores cellular, functional and organ-level homeostasis.

Copper challenge in human epithelial, fibroblast, and proliferative cell lines induced dose-dependent ROS accumulation, delayed intracellular Ca^{2+} transients, and suppression of metabolic activity. Pre-treatment with Telomir-Zn (0.1–5 μM) significantly reduced DCFH-DA ROS signals following Cu^{2+} or H_2O_2 exposure, attenuated Fluo-8–detected Ca^{2+} flux amplitude and preserved mitochondrial-associated metabolic viability. These effects were observed across cell types, consistent with modulation of labile redox-active copper pools.

In ATP7B^{-}C271X zebrafish, oral Telomir-Zn (1.5–5 ng) reduced hepatic copper levels, improved locomotor performance, normalized AST, ALT and bilirubin, attenuated hepatorenal degeneration, and significant survival in a dose-dependent manner. Histological analyses demonstrated reduced necrosis and inflammatory infiltration relative to untreated mutants.

Collectively, these findings demonstrate that intracellular copper redox modulation disrupts ROS–Ca^{2+} feedback amplification and mitigates mitochondrial-associated injury in ATP7B deficiency. Targeting labile copper-driven redox cascades may represent a mechanistically distinct strategy for restoring tissue homeostasis in copper-overload disorders.

1. Introduction

Copper is an essential transition metal required for enzymatic catalysis in cuproenzymes such as superoxide dismutase and cytochrome c oxidase. However, when present in excess or in loosely coordinated intracellular pools, copper becomes a potent redox catalyst. Labile Cu^{+}/Cu^{2+} redox cycling catalyzes Fenton-like reactions with hydrogen peroxide, generating highly reactive hydroxyl radicals (•OH) and amplifying intracellular reactive oxygen species (ROS). This redox activity promotes lipid peroxidation, oxidative DNA damage, mitochondrial membrane depolarization, and dysregulation of intracellular Ca^{2+} signaling, collectively contributing to mitochondrial dysfunction and cell injury [1–3]. Under physiological conditions, metallothioneins, glutathione, and ATP7B-mediated export constrain these labile copper

Abbreviations: ALT, Alanine aminotransferase; AST, Aspartate aminotransferase; ATP7B, ATPase copper transporting beta; Ca^{2+}, Calcium ion; Cu, Copper; DCF, 2′,7′-Dichlorofluorescein; DCFH-DA, 2′,7′-Dichlorodihydrofluorescein diacetate; dpf, Days post-fertilization; $\Delta F/F_0$, Normalized fluorescence change; EMEM, Eagle's Minimum Essential Medium; ENU, N-ethyl-N-nitrosourea; FBS, Fetal bovine serum; H_2O_2, Hydrogen peroxide; HBSS, Hanks' Balanced Salt Solution; IC_{50}, Half-maximal inhibitory concentration; LFB, Luxol Fast Blue; MMP, Mitochondrial membrane potential; MS-222, Tricaine methanesulfonate; NBF, Neutral buffered formalin; PBS, Phosphate-buffered saline; RFU, Relative fluorescence units; ROS, Reactive oxygen species; SEM, Standard error of the mean; WD, Wilson's disease; WST-1, Water-soluble tetrazolium salt-1; WT, Wild-type.

* Corresponding author at: Telomir Pharmaceuticals Inc. Miami, FL, USA.
E-mail address: angel@telomirpharma.com (I. Angel).

https://doi.org/10.1016/j.arres.2026.100168
Received 9 March 2026; Received in revised form 15 May 2026; Accepted 15 May 2026
Available online 16 May 2026

pools. When buffering capacity is exceeded, redox amplification cascades ensue [4–6].

Wilson's disease (WD) arises from loss-of-function mutations in copper-transporting ATPase ATP7B, which impair biliary copper excretion and lead to progressive hepatic copper accumulation and systemic copper toxicity [5,7]. Elevated non-ceruloplasmin-bound copper promotes oxidative stress, mitochondrial swelling, membrane permeability transition, inflammatory activation, and hepatocellular necrosis [8–10]. Increasing evidence suggests that copper-induced ROS and Ca^{2+} dysregulation form a reciprocal amplification loop that exacerbates mitochondrial dysfunction and tissue injury. While chelation strategies reduce systemic copper burden, they do not directly address intracellular redox amplification dynamics [10–12]. Current management of WD is based on lifelong reduction of systemic copper burden using copper chelators such as D-penicillamine and trientine, or by inhibiting intestinal copper absorption with zinc salts. Chelators promote urinary copper excretion, while zinc induces metallothionein in enterocytes, thereby reducing copper uptake. Although these approaches are effective in many patients, they are limited by significant drawbacks, including treatment intolerance, neurological worsening (particularly with D-penicillamine), incomplete control of hepatic and neurological disease, and poor adherence due to lifelong therapy requirements. Importantly, current therapies primarily reduce total body copper but do not directly address labile intracellular copper pools, mitochondrial dysfunction, or copper-driven redox injury [4,5].

From a treatment-development perspective, several novel agents are currently in advanced clinical or late-preclinical testing. Bis-choline tetrathiomolybdate (ALXN1840/TTM) is an oral, once-daily copper-binding compound that inhibits intestinal absorption while promoting fecal copper elimination and has demonstrated rapid normalization of copper balance and neurological improvement in Phase 2/3 studies [13]. Methanobactin (ARBM101), a bacterial-derived high-affinity copper-binding peptide, rapidly depletes hepatic copper via biliary excretion in preclinical WD models and is under evaluation for acute liver failure settings [14]. These approaches complement existing therapies and align mechanistically with intracellular redox modulation strategies such as Telomir-Zn.

The zebrafish ATP7BˆC271X model recapitulates key features of WD, including hepatic copper accumulation, locomotor impairment, and progressive tissue degeneration, providing a tractable in vivo platform for investigating copper-dependent redox injury [15,16].

Telomir-Zn was developed as a redox-modulating compound with the capacity to interact with labile intracellular metal pools. Previous unpublished studies have demonstrated that Telomir-Zn is having highest affinity to copper and iron and less so to Zinc. In prior studies, short-term exposure of HaCaT keratinocytes to Telomir-Zn rapidly increased intracellular labile zinc (DA-ZP1 probe) while producing a reciprocal, dose-dependent decrease in labile ferrous iron (FerroOrange probe). While we have not yet measured labile copper levels, these findings suggest coupled intracellular metal redistribution, whereby elevation of labile zinc is accompanied by depletion of redox-active Fe^{2+}.

Zinc is redox-inert under physiological conditions and serves structural and regulatory roles in numerous proteins. Increasing intracellular zinc while reducing labile Fe^{2+} or Cu^{2+} may decrease susceptibility to oxidative stress without broadly disrupting essential metal-dependent processes [17].

We hypothesized that modulation of redox-active copper would attenuate ROS–Ca^{2+} amplification cascades and mitigate mitochondrial-associated injury in ATP7B deficiency. To test this, we examined copper-induced ROS generation, intracellular Ca^{2+} flux, and metabolic viability in human cell systems, followed by evaluation of phenotypic and biochemical rescue in ATP7BˆC271X zebrafish.

2. Materials and methods

2.1. Chemicals

All chemicals used in this study were of analytical grade. Telomir-Zn is a zinc-complexed small molecule (2,4,6-tris(3,4-dihydro-2H-pyrrol-2-yl) pyridin. $ZnCl_2$). It was synthetized by Recipharm (Israel), with a purity of 95%.

Dimethyl sulfoxide (DMSO), agarose, Paraplast Plus, hematoxylin, eosin, and Luxol Fast Blue (Solvent Blue 38) were purchased from Sigma-Aldrich (USA). Davidson's fixative components including acetic acid and formaldehyde were obtained from SRL Chemicals and Thermo Fisher Scientific. Ethanol and xylene were obtained from SRL Chemicals (India).

Biochemical assay kits used in the study included a Copper Assay Kit (MAK127), Bilirubin Assay Kit (MAK126), and Aspartate Transaminase (AST) Assay Kit (MAK467) from Sigma-Aldrich. Alanine aminotransferase (ALT/SGPT) activity was measured using the TRUEchemie ALT Test Kit (ADX216).

2.2. Cell culture

HaCaT keratinocytes (AddexBio, T0020001), MRC-5 human fetal lung fibroblasts (ATCC CCL-171), and PC-3 prostate carcinoma cells (ATCC CRL-1435) were cultured at 37 °C in a humidified incubator with 5% CO_2. PC-3 cells were maintained in F-12 K medium, HaCaT cells in DMEM supplemented with 2 mM sodium pyruvate, and MRC-5 cells in EMEM. All media were supplemented with 10% fetal bovine serum (FBS) and 1% penicillin–streptomycin.

Cells were maintained in logarithmic growth phase and used within standardized passage ranges. For viability assays, cells were seeded in 96-well plates at densities of 8×10^3 cells per well for PC-3 and MRC-5 cells, and 1.7×10^4 cells per well for HaCaT cells, in 150 μL complete medium. Cells were allowed to adhere for 24 h prior to treatment.

2.3. Copper-Induced cytotoxicity and viability assessment

Cells were treated with $CuCl_2$ at final concentrations of 35–200 μM for 48 h. Following exposure, cellular morphology was assessed by light microscopy. Metabolic activity was quantified using the WST-1 assay according to the manufacturer's instructions. Absorbance was measured using a CLARIOstar microplate reader (BMG Labtech), and cell viability was expressed relative to untreated controls following background subtraction.

Each condition was assessed with three independent biological replicates.

2.4. Redox challenge and ROS quantification

Cells were pre-treated with Telomir-Zn (0.1–5 μM) for 1 h prior to oxidative challenge. Copper-induced redox stress was initiated using $CuCl_2$ (10–100 μM), and peroxide challenge was performed using H_2O_2 (1 mM).

Intracellular reactive oxygen species (ROS) levels were quantified using the fluorescent probe DCFH-DA (2′,7′-dichlorodihydrofluorescein diacetate). Cells were incubated with DCFH-DA for 30 min at 37 °C, washed with HBSS, and fluorescence measurements were obtained immediately following oxidant challenge and continuously monitored for up to 70 min. Fluorescence intensity was recorded using a CLARIOstar microplate reader (BMG Labtech) and expressed relative to untreated controls.

Each condition was assessed with three independent biological replicates.

2.5. Intracellular calcium flux analysis

HaCaT cells were seeded to near-confluence and treated with Telomir-Zn (0.1–5 μM) for 1 h at 37 °C. Cells were then equilibrated in Hanks' Balanced Salt Solution (HBSS) supplemented with 0.1 mM Ca^{2+} and 20 mM HEPES in order to detect intracellular Ca^{2+} release rather than influx from media.

Intracellular Ca^{2+} dynamics were monitored using the fluorescent indicator Fluo-8 AM (5 μg/mL) in the presence of 2.5 mM probenecid to enhance dye retention. Cells were incubated with Fluo-8 AM for 1 h at 37 °C prior to oxidant challenge. Following dye loading, cells were challenged with Cu^{2+} (50 or 200 μM), Fe^{2+} (200 μM), or H_2O_2 (0.2–1 mM).

Rapid calcium responses (0–2 min) were measured using automated reagent injection, followed by extended kinetic monitoring for up to 45 min. Fluorescence changes were expressed as F/F_0.

2.6. Zebrafish husbandry and ethical compliance

Wild-type (WT) and ATP7BˆC271X homozygous mutant zebrafish (Danio rerio) were bred and maintained under standardized laboratory conditions (27 ± 1 °C; pH 7.2–7.4; 14 h light/10 h dark photoperiod) in an AAALAC-accredited facility. All experimental procedures were conducted in accordance with institutional animal care guidelines and approved by the Committee for the Purpose of Control and Supervision of Experiments on Animals (CPCSEA), Government of India (Approval No PENT015, dated July 19th, 2025).

2.7. Generation of ATP7BˆC271X mutants

ATP7B mutant zebrafish were generated using ENU-mediated forward genetic mutagenesis [18]. Stable heterozygous founders were intercrossed to obtain homozygous ATP7BˆC271X −/− larvae (Gene ID: 556,499), resulting in a truncation at amino acid 271 of the ATP7B protein.

Mutant larvae were initially screened at 3 days post-fertilization (dpf) for characteristic behavioral phenotypes, including impaired touch response and restricted body bending. Larvae displaying the expected mutant phenotype were selected and confirmed prior to inclusion in subsequent experimental studies.

2.8. Group allocation

At 5 days dpf, larvae were randomized into four experimental groups (n = 66 per group): (1) wild-type (WT) control; (2) ATP7BˆC271X −/− untreated mutant control; (3) ATP7BˆC271X −/− treated with Telomir-Zn (1.5 ng); and (4) ATP7BˆC271X −/− treated with Telomir-Zn (5 ng).

2.9. Dosing regimen

The working stocks of the test compounds were prepared by solubilizing with a mixture of Test candidate (98%), Commercial feed (TetraBits) (1%), and Phenol Red marker (0.3%), Sterile water (0.7%). Zebrafish larvae aged 5 to 18 days post-fertilization (dpf) were subjected to oral gavage for the administration of test compound. The gavage solution comprised 98% test candidate, 0.3% phenol red (to aid visualization), and 1% commercial fish feed (to enhance palatability), Sterile water to reconstitute to desired consistency (0.7%). Two dosage concentrations, 1.5 ng and 5 ng per larva, were prepared. A total volume of 5 nanoliters (nl) of the gavage solution was delivered per larva using a WPI PicoPump system fitted with a fine-tipped glass capillary, which was pulled and beveled to accommodate the larval mouth size. Larvae were anesthetized in 0.016% Tricaine (MS-222) prior to gavage to facilitate immobilization and reduce handling stress. The solution was administered via gentle, controlled flow to prevent regurgitation or injury. Care was taken to avoid introducing air bubbles into the capillary or the gastrointestinal tract.

2.10. Behavioral and biochemical screening

Comprehensive phenotypic screening was performed at 19 dpf Behavioral endpoints included episodic tremor frequency, maze exploratory latency, light/dark preference, swim distance and velocity, and ataxia assessment based on bend frequency and turn angle. Locomotor tracking parameters were quantified using ImageJ-based motion analysis.

Histological evaluation was performed using hematoxylin and eosin (H&E) and Luxol Fast Blue (LFB) staining on paraffin-embedded sections (5–7 μm thickness). Hepatic copper levels were quantified using a colorimetric copper assay kit (Sigma-Aldrich MAK127; absorbance measured at 359 nm). Liver injury biomarkers including alanine aminotransferase (ALT), aspartate aminotransferase (AST), and bilirubin were measured using commercially available assay kits. Survival outcomes were evaluated using Kaplan–Meier survival analysis.

For biochemical analyses, liver samples were pooled (n = 6 larvae per pool), with three pools analyzed per experimental group.

2.10.1. Drug screening

Following completion of the dosing regimen, phenotypic and biochemical screening was performed at 19 dpf. Assessments included behavioral analysis, histopathological evaluation, and biochemical measurements to evaluate physiological and tissue-level responses to treatment.

2.10.2. Episodic tremor events

Episodic tremor events were used as an indicator of neuromotor dysfunction in zebrafish larvae. At 19 dpf. larvae were placed individually in wells of a multi-well plate and allowed to acclimate for 3 ± 1 min prior to observation. Larval movements were recorded using a high-resolution camera mounted on a microscope system connected to a computer for video capture. Video recordings were analyzed to quantify the frequency and duration of tremor events, defined as rhythmic involuntary shaking movements. Tremor frequency was calculated as the number of events per observation period for each larva.

2.10.3. Exploratory performance for cognitive capacity-maze experiment tank

Exploratory navigation behavior was assessed using a maze tank containing multiple pathways. At 19 dpf, Individual larvae were placed at the pre-start position and allowed to acclimate for 5 min. Following acclimation, larvae were positioned at the maze starting point and allowed to freely explore the maze for up to 5 min. Larval movements were recorded using video tracking. The primary endpoint measured was latency to reach the terminal zone of the maze. Latency values were extracted from video recordings for each larva and used for comparative analysis between study groups.

2.10.4. Light/Dark

Anxiety-like behavior was evaluated using a light/dark (L/D) preference assay. The experimental arena consisted of a recording tank divided into two zones with contrasting illumination (light and dark). At 19 dpf, Individual larvae were placed in the tank and allowed to acclimate for 10–15 min prior to testing. Following acclimation, larvae were introduced into the center of the arena and allowed to freely explore both zones for 5–10 min. Movements were recorded using video tracking, and time spent in each zone and movement patterns were quantified for subsequent analysis

2.10.5. Swim distance and swim velocity

Locomotor activity was evaluated using an open-field assay. At 19 dpf, Individual zebrafish larvae (N = 24) were placed in the recording arena, and movements were captured using video tracking. Raw

movement tracks were extracted from video files and processed using ImageJ software to obtain x–y coordinate data for each frame.

Coordinate data were exported in CSV format and analyzed to calculate locomotor parameters. Pixel coordinates were converted to millimeter units, and cumulative swim distance per minute was calculated from frame-by-frame displacement. Swim velocity was determined by dividing total distance traveled by time over the recording period. These parameters were used to quantify locomotor performance across study groups.

2.10.6. Ataxia stereotype

Motor coordination was evaluated by quantifying bend frequency during spontaneous locomotion. At 19 dpf, Individual larvae were transferred to separate wells of a multi-well plate and allowed to acclimate for 15 min prior to recording. Larval movements were then recorded using a video imaging system over a defined observation period.

Video recordings were analyzed using behavioral tracking software to quantify the number of body bends per minute. Bend frequency was calculated from frame-by-frame analysis of larval movement and used as a quantitative indicator of motor coordination.

2.10.7. Histology-kidney

Histopathological evaluation of zebrafish larvae kidney and liver tissues was performed to assess disease progression and treatment-associated tissue protection. At 19 days dpf, following completion of the dosing regimen, larvae from each experimental group (n = 6) were collected for histological analysis.

Larvae were euthanized using tricaine methane sulfonate (MS-222) and immediately fixed to preserve tissue morphology. Whole larvae were immersed in 5% neutral buffered formalin (NBF) for 4–8 h. Following fixation, samples were dehydrated through a graded ethanol series (70–100%) and embedded in paraffin. Paraffin-embedded tissues were sectioned at 5–7 μm thickness using a microtome (Abron Scientific Advanced Microtomy AB-91–07).

Tissue sections were stained using hematoxylin and eosin (H&E) and Luxol Fast Blue (LFB). Histological sections were examined using light microscopy at 20 × and 40 × magnification, and images were captured using a Labomed digital imaging system.

Pathological changes were evaluated using a semi-quantitative scoring system to assess the degree of tissue degeneration:

- **Grade 0 (Normal):** No visible signs of tissue degeneration
- **Grade 1 (Mild degeneration):** Slight cellular swelling, minor vacuolization, or rare apoptotic cells
- **Grade 2 (Moderate degeneration):** Cellular disorganization, increased vacuolization, partial loss of cellular integrity, and inflammatory infiltration
- **Grade 3 (Severe degeneration):** Extensive tissue damage, necrosis, pronounced inflammatory response, and marked structural disruption
- **Grade 4 (Complete degeneration):** Near-total loss of normal tissue architecture with widespread necrosis or fibrosis

2.10.8. Histology-liver

Histopathological evaluation of zebrafish larval liver tissue was performed to assess disease progression and treatment-associated tissue protection across all experimental groups. At 19 dpf, following completion of 14 doses of the test compounds, larvae from each study group (n = 6) were collected for histological analysis.

Larvae were euthanized using tricaine methane sulfonate (MS-222) and immediately fixed to preserve tissue morphology. Whole larvae were immersed in 5% NBF for 4–8 h. Following fixation, tissues were dehydrated through a graded ethanol series (70–100%) and embedded in paraffin. For optimal visualization of hepatic structures, larvae were positioned in a left lateral orientation prior to embedding.

Paraffin-embedded samples were sectioned at 5–7 μm thickness using a microtome (Abron Scientific Advanced Microtomy AB-91–07) and stained with H&E and LFB. Tissue sections were examined using light microscopy at 20 × and 40 × magnification, and images were captured using a Labomed digital imaging system.

Histopathological scoring was performed to quantify the degree of hepatic degeneration across treatment groups. Digital images were analyzed using the QuPath software platform to identify and quantify degenerative changes according to the predefined pathology scoring criteria described above.

2.10.9. Copper in dry liver tissue

Hepatic copper levels were quantified using a colorimetric copper assay kit (Sigma-Aldrich, MAK127) according to the manufacturer's instructions. Liver tissues were isolated from zebrafish larvae and pooled (n = 6 larvae per pool; three pools per experimental group) in 0.9% saline solution. Samples were homogenized and processed for copper measurement.

Briefly, liver homogenates were mixed with assay reagents containing a chromogenic probe that forms a colored complex with copper ions. Following incubation at room temperature in the dark for 5 min, absorbance was measured at 359 nm using a microplate reader. Copper concentrations were calculated using a standard calibration curve generated from kit-provided standards. The assay detection range was 7 μg/dL (1.0 μM) to 300 μg/dL (47 μM).

2.10.10. ALT (Alanine transaminase)

ALT activity was measured in pooled zebrafish liver samples to assess hepatic injury. Liver tissues were dissected from anesthetized larvae under a stereomicroscope, pooled, and immediately placed on ice. Samples were homogenized in cold phosphate-buffered saline (PBS, pH 7.4) using a micro-homogenizer (n = 6 larvae per pool; three pools per experimental group) and centrifuged at 10,000 × g for 10 min at 4 °C to remove cellular debris. The resulting supernatant was collected for enzymatic analysis.

ALT activity was quantified using the TRUEchemie ALT (SGPT) Test Kit according to the manufacturer's instructions. Tissue lysates were incubated with the working reagent mixture (R1:R2, 4:1), and enzymatic activity was measured kinetically at 340 nm using a microplate reader. ALT activity was calculated using the manufacturer-provided calibration factor and expressed as units per liter (U/L) of tissue lysate.

2.10.11. AST (Aminotransferase)

AST activity was measured in pooled zebrafish liver samples to assess hepatic injury. Liver tissues were isolated from larvae and pooled (n = 6 larvae per pool; three pools per experimental group) in 0.9% saline. Samples were homogenized and processed for enzymatic analysis.

AST activity was quantified using a commercial assay kit (Sigma-Aldrich, MAK467) according to the manufacturer's instructions. The assay is based on the enzymatic generation of oxaloacetate by AST, coupled to NADH oxidation. Samples and standards were incubated with the working reagent, and the decrease in NADH absorbance was monitored kinetically at 340 nm. Enzyme activity was calculated from the rate of NADH consumption and expressed as U/L of tissue lysate.

2.10.12. Total bilirubin

Total bilirubin levels were measured in pooled zebrafish liver samples to assess hepatic dysfunction. Liver tissues were isolated from larvae and pooled (n = 6 larvae per pool; three pools per experimental group) in 0.9% saline and homogenized for analysis.

Total bilirubin was quantified using a commercial bilirubin assay kit (Sigma-Aldrich, MAK126) according to the manufacturer's instructions. The assay is based on the Jendrassik–Grof reaction, in which bilirubin reacts with diazotized sulfanilic acid to form a colored complex. Following incubation with the assay reagents, absorbance was measured at 530 nm using a microplate reader. Bilirubin concentrations were

calculated using kit-provided calibration standards.

2.11. Statistical analysis

Data are presented as mean ± SEM. Statistical comparisons were performed using one-way or two-way ANOVA along with post-hoc Tukey's test. Significant differences were assessed at p values of $p < 0.05$ (*), $p < 0.01$ (**), $p < 0.001$ (***) and $p < 0.0001$(****). Value (ns) was considered non-significant. Kaplan–Meier survival curves were analyzed using the log-rank test.

3. Results

3.1. Copper exposure induces concentration-dependent cytotoxicity in human cell lines

To characterize copper-induced cellular vulnerability, HaCaT keratinocytes, PC-3 prostate carcinoma cells, and MRC-5 fibroblasts were exposed to $CuCl_2$ (35–200 μM) for 48 h. Copper treatment resulted in a concentration-dependent reduction in metabolic viability as measured by WST-1 assay (Fig. 1).

HaCaT and PC-3 cells demonstrated marked sensitivity to copper exposure, with greater than 20% reduction in viability observed at 35 μM, and >60% suppression at 200 μM. In contrast, MRC-5 fibroblasts exhibited relative resistance at lower concentrations, maintaining >95% viability up to 100 μM, but declined to 82 ± 1% at 200 μM.

Morphological assessment by light microscopy revealed concentration-dependent cellular alterations, including cytoplasmic granulation, membrane blebbing, and detachment in copper-sensitive cell lines. These findings confirm differential cellular susceptibility to copper-induced cytotoxic stress and establish a concentration range suitable for subsequent redox and calcium flux analyses.

3.2. Telomir-Zn attenuates copper-induced ROS amplification

To determine whether modulation of labile copper pools alters oxidative stress dynamics, intracellular ROS levels were quantified in HaCat cells using DCFH-DA following copper or peroxide challenge. Exposure to $CuCl_2$ (10–100 μM) induced concentration-dependent ROS elevation, with fluorescence increase peaking between 30 and 60 min and continuing to increase through 75 min. At 100 μM copper, ROS levels increased approximately 2.5 ± 0.3-fold relative to baseline ($p < 0.01$). Hydrogen peroxide (1 mM) produced a comparable oxidative response (Fig. 2).

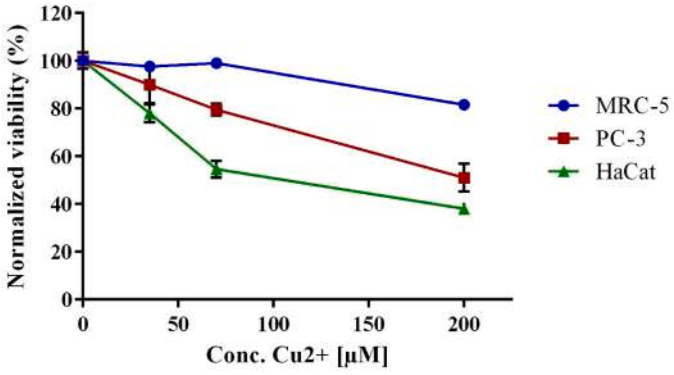

Fig. 1. Copper induces concentration-dependent cytotoxicity in human cell lines.
HaCaT, PC-3, and MRC-5 cells were exposed to $CuCl_2$ (35–200 μM) for 48 h, and metabolic viability was assessed by WST-1 assay. Data are expressed as relative absorbance (450 nm) normalized to untreated controls. Copper exposure resulted in dose-dependent reduction in viability, with Keratinocyte and prostate cancer cell lines exhibiting greater sensitivity compared to fibroblasts. Values represent mean ± SD from independent biological replicates (n = 3).

Pre-treatment with Telomir-Zn (0.1–5 μM) significantly reduced ROS accumulation following both copper and H_2O_2 challenge. In cells exposed to 10 μM Cu^{2+}, 0.5 μM Telomir-Zn reduced ROS signals to levels comparable to untreated controls. Similarly, 5 μM Telomir-Zn attenuated peroxide-induced ROS elevation to near-baseline values.

Similar attenuation of copper-induced ROS signals was observed across primary fibroblasts, as well as epithelial- and keratinocyte cell lines.

3.3. Telomir-Zn attenuates copper-induced intracellular Ca^{2+} dysregulation

To evaluate the impact of copper-induced redox stress on calcium signaling, intracellular Ca^{2+} dynamics were assessed in confluent HaCaT cells using Fluo-8 fluorescence imaging. Cells were equilibrated in Hanks' Balanced Salt Solution (HBSS) supplemented with minimal Ca^{2+} (0.1 mM Ca^{2+}) in order to detect intracellular Ca^{2+} release rather than influx of extracellular Ca^{2+}. Acute Cu^{2+} challenge (50–200 μM) produced a biphasic response characterized by initial signal quenching within 0–2 min, followed by delayed Ca^{2+} elevation peaking between 5 and 15 min post-challenge (Fig. 3). At 200 μM copper, peak F/F_0 reached 1.8 relative to baseline.

Pre-treatment with Telomir-Zn (0.1–5 μM, 1 h) significantly reduced copper-induced Ca^{2+} flux amplitude. At 5 μM, peak F/F_0 was reduced to <1. Suppression of calcium transients was observed at both 50 and 200 μM copper challenge concentrations.

These findings indicate that modulation of redox-active copper pools attenuates calcium amplification following oxidative challenge, consistent with disruption of ROS–Ca^{2+} feedback signaling.

3.4. Telomir-Zn improves neuromotor performance in ATP7BˆC271X zebrafish

To evaluate functional consequences of copper dysregulation in vivo, locomotor behavior was assessed in ATP7BˆC271X mutant zebrafish larvae (19 days post-fertilization). Mutant larvae exhibited significantly increased episodic tremor frequency compared with wild-type controls (0 ± 0 Average No of events/min vs. 5.12±1.25 Average No of events/min ; $p < 0.001$). In addition, total swim distance and velocity were reduced to 103.4 ± 22.85 distance travelled/min and 241.5 ± 31.36 distance travelled/min of wild-type levels, respectively ($p < 0.01$), accompanied by elevated *ataxia* stereotype (No of bends/ min 2.95 ±2.07 vs. 18.37±6.15 in wild-type; $p < 0.001$) (Figs. 4–6).

Oral administration of Telomir-Zn (1.5 ng or 5 ng) significantly improved motor parameters in a dose-dependent manner. The 1.5 ng dose partially restored swim distance 134.9 ± 13.07 distance travelled/min vs. untreated mutants; $p < 0.05$), whereas the 5 ng dose produced more pronounced improvement in both distance and velocity (220.9 ± 41.48 distance travelled/min vs. untreated mutants; $p < 0.001$). Tremor frequency was correspondingly reduced in treated groups. Exploratory behavior analysis demonstrated reduced thigmotaxis and improved movement regularity in Telomir-Zn–treated larvae.

These findings indicate that modulation of copper-associated redox stress is associated with functional improvement in ATP7B-deficient zebrafish Fig. 5.

3.5. Telomir-Zn reduces hepatic copper accumulation in ATP7BˆC271X zebrafish

To determine whether functional improvement was associated with altered tissue copper burden, hepatic copper levels were evaluated. ATP7BˆC271X mutants exhibited significant hepatic copper accumulation compared with wild-type controls, with 2.83±0.41 increase based on histological scoring and 271.6 ± 16.19 ng/mg increase in liver copper concentration (Fig. 7).

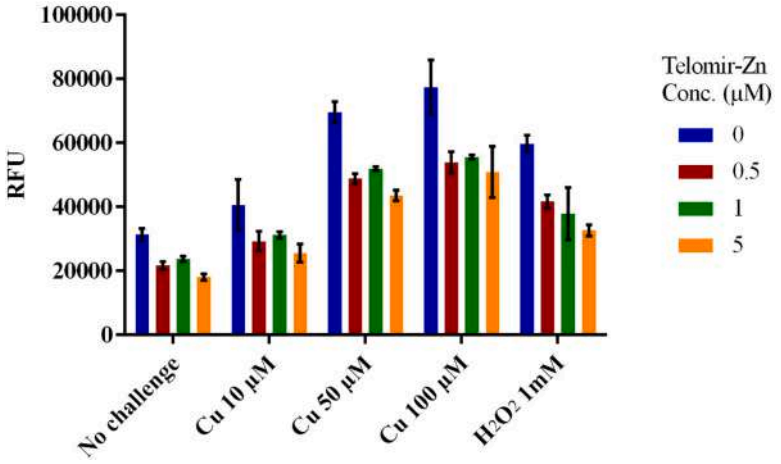

Fig. 2. Telomir-Zn attenuates copper- and peroxide-induced ROS generation.
Intracellular ROS levels were measured using DCFH-DA following challenge with $CuCl_2$ (10–100 μM) or H_2O_2 (1 mM) in the presence or absence of Telomir-Zn (0.1–5 μM). Fluorescence intensity was monitored over 60–75 min and expressed as relative fluorescence units (RFU). Copper exposure induced dose-dependent ROS amplification, which was significantly reduced by Telomir-Zn pre-treatment. Data represent mean ± SD from independent biological replicates (n = 3).

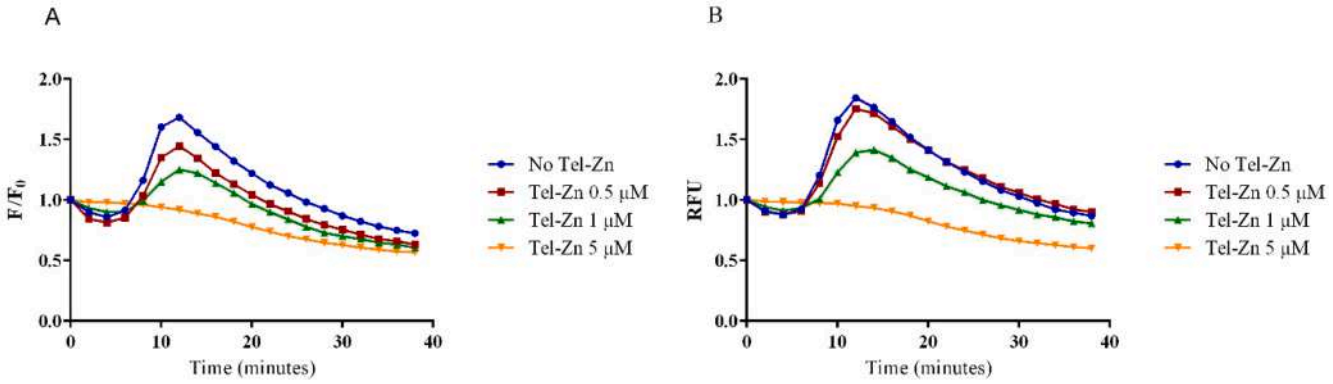

Fig. 3. Telomir-Zn attenuates copper-induced intracellular Ca^{2+} dysregulation.
Representative Fluo-8 fluorescence traces showing intracellular Ca^{2+} dynamics following Cu^{2+} challenge at 50 μM (A) and 200 μM (B) in HaCaT cells. Copper exposure produced delayed Ca^{2+} elevation after initial signal quenching. Pre-treatment with Telomir-Zn (0.1–5 μM) reduced peak F/F_0 amplitude.

Oral Telomir-Zn administration reduced hepatic copper burden in a dose-dependent manner. Treatment with 1.5 ng decreased hepatic copper levels by 149.6 ± 0.57 ng/mg ($p < 0.05$ vs. untreated mutants), while 5 ng reduced levels by 137.6 ± 1.15 ng/mg($p < 0.001$). Renal histological scoring was also significantly reduced in treated groups ($p < 0.01$).

These findings indicate that modulation of redox-active copper pools is associated with reduced tissue copper accumulation in ATP7B-deficient zebrafish.

3.6. Telomir-Zn reduces biochemical markers of hepatic injury

To assess hepatic injury, alanine aminotransferase (ALT), aspartate aminotransferase (AST), and total bilirubin levels were measured. ATP7BˆC271X mutants exhibited significantly elevated ALT (120.7 ± 8.5 U/L), AST (120.7 ± 8.5 U/L), and bilirubin (1.08±1.01 mg/dL) compared with wild-type controls ($p < 0.001$) (Fig. 8).

Telomir-Zn treatment reduced these injury markers in a dose-dependent manner. At 5 ng, ALT levels decreased to 59±4 U/L ($p < 0.001$ vs. untreated mutants), with corresponding reductions in AST and bilirubin. The AST/ALT ratio normalized toward WT levels (0 WT vs 12 mutant; reduced to 6 at 5 ng). These findings indicate attenuation of biochemical indices of hepatic injury in ATP7B-deficient zebrafish following Telomir-Zn administration.

3.7. Telomir-Zn attenuates hepatorenal histopathological degeneration

Histological analysis of hematoxylin and eosin (H&E)–stained sections (400 × magnification) revealed marked tissue degeneration in ATP7BˆC271X mutants. Mutant larvae exhibited Grade 3 pathology characterized by extensive hepatocellular necrosis, cytoplasmic vacuolization, inflammatory infiltration, and structural disorganization.

In the kidney, the wild-type (WT) larvae exhibited Grade 0 (Normal) histology, with well-preserved glomerular and tubular architecture, and no signs of degeneration. In contrast, the ATP7B - C271X -/- mutant group showed Grade 3 (Severe Degeneration), characterized by extensive tubular necrosis, cellular disintegration, and a marked inflammatory response. Treatment with Telomir-Zn at 1.5 ng led to partial restoration of renal structure, corresponding to Grade 2 (Moderate Degeneration), with improved tissue organization and reduced necrosis, with signs of inflammation. Notably, the higher dose of Telomir-Zn (5 ng) resulted in substantial pathological improvement, classified as Grade 1 (Mild Degeneration), with near-normal tubular morphology and only minor cellular alterations, indicating effective renal protection and structural recovery in a dose-dependent manner (Fig. 9 Top).

Telomir-Zn treatment reduced histopathological severity in a dose-dependent manner. Larvae treated with 1.5 ng demonstrated Grade 2 pathology, with partial preservation of hepatic architecture and reduced vacuolization. Treatment with 5 ng further reduced histological severity

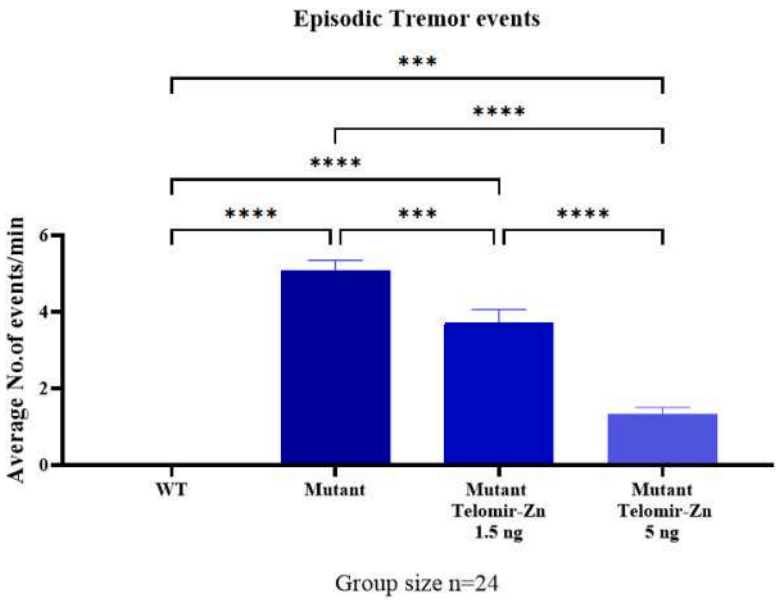

Fig. 4. Neuromotor deficits in ATP7BˆC271X zebrafish and dose-dependent improvement following Telomir-Zn treatment.
Episodic tremor frequency (events/min) in wild-type, ATP7BˆC271X mutant, and Telomir-Zn–treated larvae (1.5 ng and 5 ng). Mutant larvae exhibited significantly increased tremor frequency relative to wild-type controls. Telomir-Zn treatment reduced tremor events in a dose-dependent manner. Data are presented as mean ± SEM. Statistical comparisons were performed using one-way ANOVA with post hoc testing as described in Methods.

to Grade 1, characterized by minimal cellular swelling and limited inflammatory infiltration (Fig. 9). Quantitative analysis indicated a 64% reduction in necrotic area and a 58% reduction in inflammatory infiltration at 5 ng ($p < 0.01$ vs. untreated mutants) (Fig. 10).

These findings demonstrate attenuation of copper-associated tissue degeneration in ATP7B-deficient zebrafish following Telomir-Zn administration.

3.8. Telomir-Zn improves survival in ATP7BˆC271X zebrafish

Survival was evaluated using Kaplan–Meier analysis. ATP7BˆC271X mutants demonstrated reduced survival compared with wild-type controls over the observation period. Telomir-Zn treatment improved survival probability in a dose-dependent manner, with the 5 ng group showing greater survival benefit relative to untreated mutants (Fig. 11). Statistical comparison of survival curves was performed using the log-rank test as described in Methods.

4. Discussion

This study demonstrates that modulation of labile copper pools attenuates copper-driven redox amplification and is associated with functional improvement in ATP7B deficiency. In human cell systems, copper exposure induced concentration-dependent ROS accumulation and delayed intracellular Ca^{2+} elevation, consistent with Fenton-type redox cycling and ROS–Ca^{2+} feedback amplification. Telomir-Zn reduced oxidant-induced ROS signals and suppressed delayed calcium transients, supporting a role in regulating redox-active intracellular copper dynamics.

Copper toxicity is mediated in part by non-ceruloplasmin-bound Cu catalyzing ROS generation through redox cycling, overwhelming glutathione and metallothionein buffering systems and promoting mitochondrial dysfunction [19,20]. Disruption of mitochondrial membrane potential and permeability transition contributes to hepatocellular injury in WD. In addition, recent studies have identified cuproptosis, a form of copper-dependent regulated cell death characterized by copper binding to lipoylated mitochondrial TCA cycle proteins and destabilization of Fe–S cluster enzymes. This process induces mitochondrial proteotoxic stress and metabolic collapse. Although the link between intracellular copper redistribution and disruption of the ROS–Ca^{2+} amplification loop remains primarily correlative, emerging evidence supports the central role of redox-active metals in sustaining reciprocal ROS-calcium crosstalk and mitochondrial injury. Recent studies demonstrate that targeted modulation of intracellular redox homeostasis through copper dysregulation can effectively disrupt oxidative stress signaling and downstream cell death pathways. These findings reinforce the mechanistic plausibility that attenuation of labile copper pools, as achieved with Telomir-Zn, can interrupt self-amplifying ROS–Ca^{2+} cascades and mitigate copper-driven pathology in ATP7B deficiency [21,22].

In WD, mitochondrial copper accumulation and respiratory chain dysfunction are well documented, suggesting that copper-mediated mitochondrial injury may share mechanistic features with cuproptosis. Such processes may further amplify ROS generation and calcium dysregulation, contributing to hepatocellular damage in ATP7B deficiency [22,23]. The observed attenuation of ROS and Ca^{2+} amplification suggests that intracellular copper modulation may limit redox-driven signaling cascades that exacerbate mitochondrial stress. Although direct measurements of mitochondrial membrane potential were not performed, preservation of metabolic viability and reduction in calcium dysregulation are consistent with mitigation of oxidative injury.

In the ATP7BˆC271X zebrafish model, copper accumulation was associated with locomotor impairment, elevated transaminases, histopathological degeneration, and reduced survival. Telomir-Zn treatment reduced hepatic copper burden and improved behavioral, biochemical, and histological parameters in a dose-dependent manner. These findings support the concept that targeting redox-active copper pools may influence both molecular and organ-level outcomes in ATP7B deficiency.

Current therapeutic strategies in WD primarily focus on reducing systemic copper burden through chelation or zinc-mediated absorption blockade [24,25]. However, intracellular redox amplification may persist despite reductions in total copper load. The present findings raise the possibility that modulation of labile copper-driven redox cycling and intracellular zinc replacement may represent a complementary mechanistic approach distinct from bulk copper depletion. Further studies are required to directly demonstrate copper zinc replacement and to determine how intracellular copper redistribution interfaces with ATP7B trafficking and mitochondrial regulation.

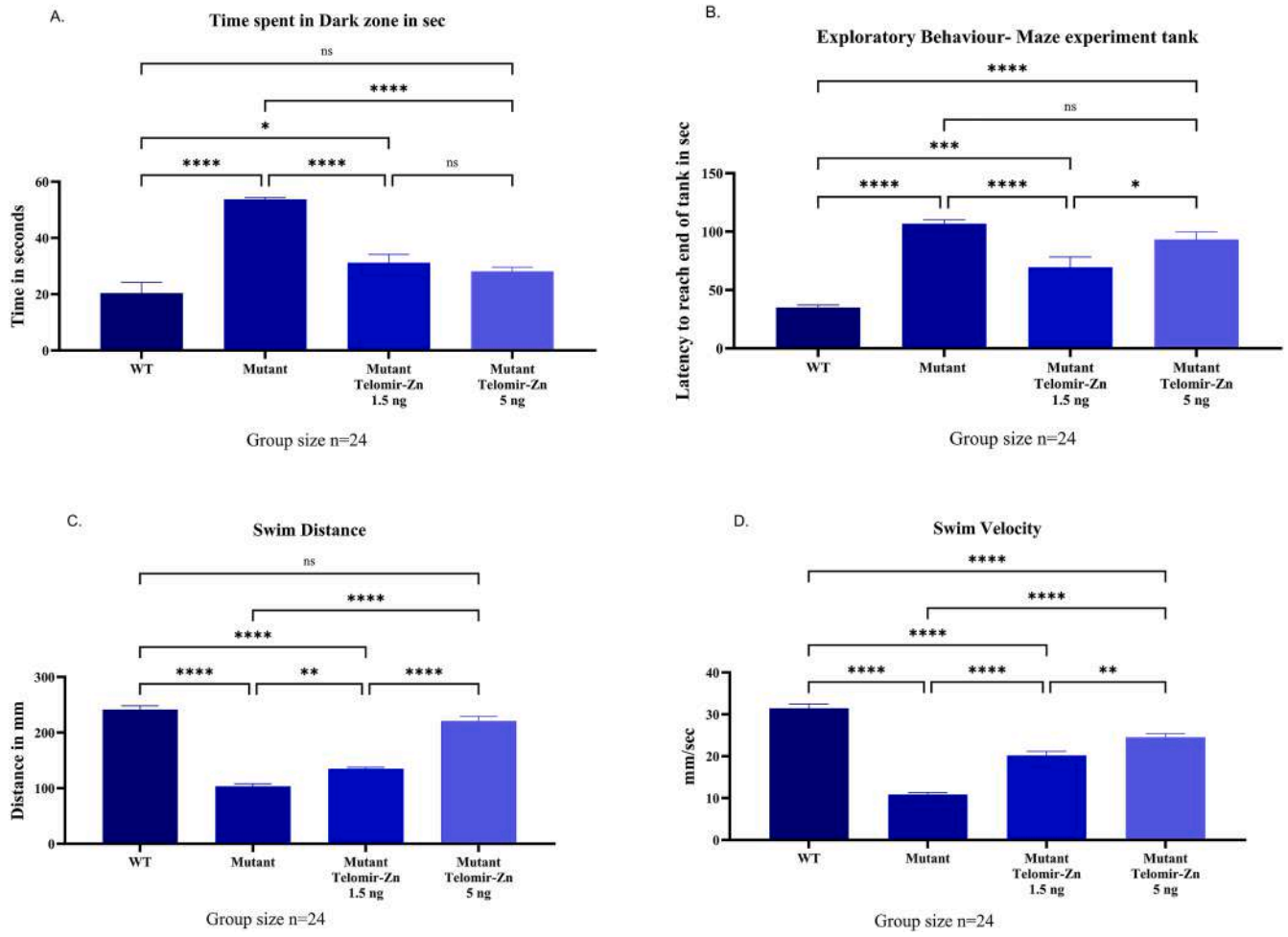

Fig. 5. Telomir-Zn improves locomotor activity patterns in ATP7BˆC271X zebrafish.
Quantitative assessment of locomotor parameters in wild-type, ATP7BˆC271X mutant, and Telomir-Zn–treated larvae. (A) Light/dark preference testing. (B) Exploratory behavior profiles derived from swim tracking analysis. (C) Total swim distance. (D) Swim velocity. ATP7BˆC271X mutants exhibited impaired movement dynamics and altered exploratory behavior relative to wild-type controls. Telomir-Zn treatment improved locomotor performance and movement regularity in a dose-dependent manner. Representative swim tracking heat maps illustrate spatial exploration patterns across groups. Data are presented as mean ± SEM. Statistical analyses were performed as described in Methods.

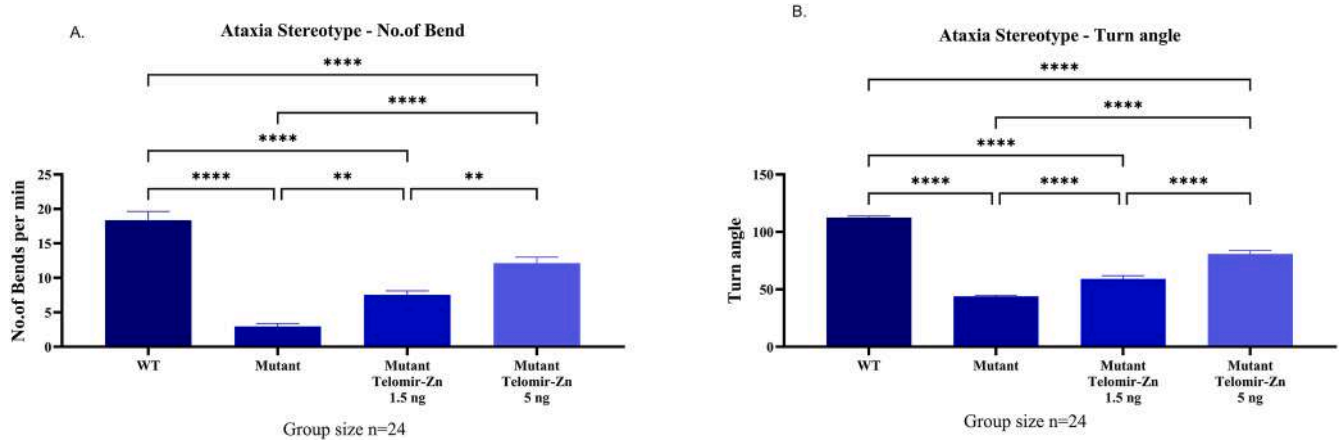

Fig. 6. Telomir-Zn improves ataxia-associated behavioral parameters in ATP7BˆC271X zebrafish.
(A) Quantification of exploratory band crossings as a measure of locomotor range. (B) Analysis of turn angles reflecting movement coordination. ATP7BˆC271X mutants exhibited reduced exploratory activity and increased thigmotaxis relative to wild-type controls. Telomir-Zn treatment improved locomotor coordination and exploratory range, with greater effects observed at 5 ng. Data are presented as mean ± SEM. Statistical comparisons were performed as described in Methods.

Several limitations warrant consideration. In vitro experiments were limited to acute exposure paradigms, which may not fully capture

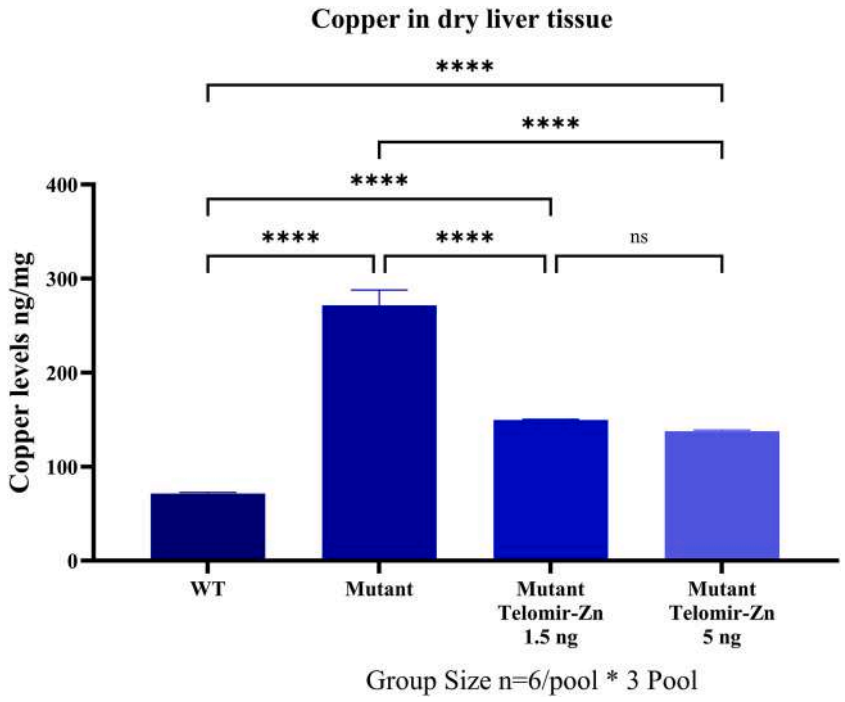

Fig. 7. Telomir-Zn reduces copper levels in the liver of ATP7Bˆ C271X zebrafish.
Quantification of liver copper levels. ATP7Bˆ C271X mutants exhibited elevated tissue copper accumulation relative to wild-type controls. Telomir-Zn treatment reduced hepatic and renal copper burden in a dose-dependent manner. Data are presented as mean ± SEM. Statistical comparisons were performed as described in Methods.

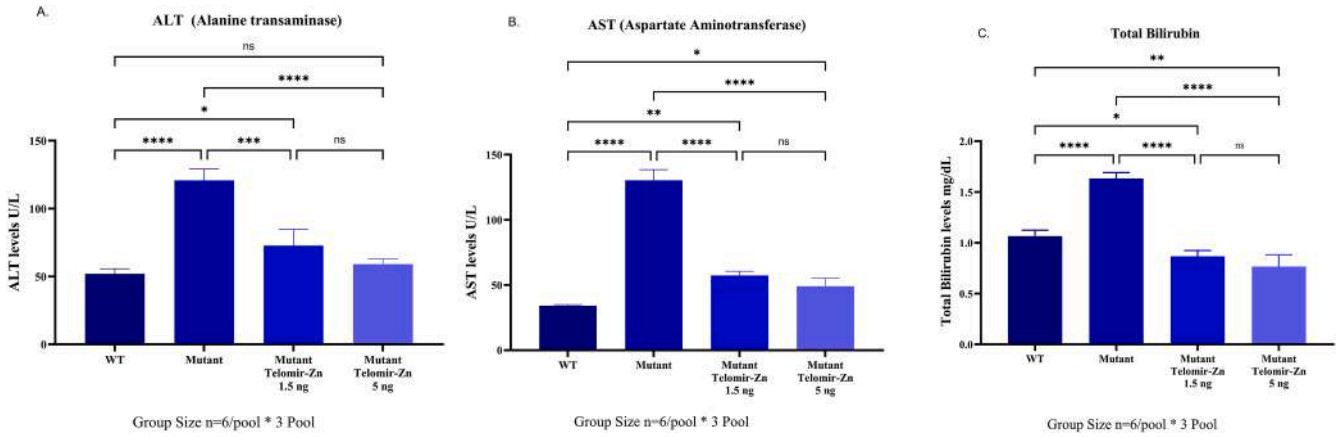

Fig. 8. Telomir-Zn reduces markers of hepatic injury in ATP7Bˆ C271X zebrafish.
(A) Alanine aminotransferase (ALT). (B) Aspartate aminotransferase (AST). (C) Total bilirubin levels. ATP7Bˆ C271X mutants exhibited elevated biochemical markers of liver injury relative to wild-type controls. Telomir-Zn treatment reduced injury markers in a dose-dependent manner. Data are presented as mean ± SEM. Statistical analyses were performed as described in Methods.

chronic redox remodeling. Direct measurements of mitochondrial membrane potential, oxidative phosphorylation, and ATP7B trafficking were not performed. Additionally, while the zebrafish model recapitulates key aspects of copper overload, differences in hepatobiliary architecture and physiology limit extrapolation to mammalian systems. Future studies incorporating mammalian models and mitochondrial functional assays incorporating mitochondrial ROS measurements, mitochondrial membrane potential assays, and ATP production analysis will further define the mechanistic scope of intracellular copper modulation and will further clarify how intracellular copper redistribution influences mitochondrial redox homeostasis. To partially address an issue of potential off-target or general antioxidant effects, we note that Telomir-Zn was well tolerated in the ATP7Bˆ C271X mutant background across the tested dose range (1.5–5 ng), with no overt signs of toxicity, changes in general morphology, or increased mortality compared with untreated mutants. Nevertheless, a dedicated wild-type (WT) + Telomir-Zn control group was not included in the present study, primarily due to logistical constraints on animal usage and the focus of this proof-of-concept investigation on phenotypic rescue in the disease model. Future studies in wild-type zebrafish or mammalian models of copper overload will incorporate the WT + Telomir-Zn arm to fully exclude nonspecific effects and to further delineate disease-specific versus general actions of the compound.

The quantitative rescue observed across behavioral, biochemical, and histopathological endpoints demonstrates that redox-active copper modulation translates into measurable functional recovery in vivo.

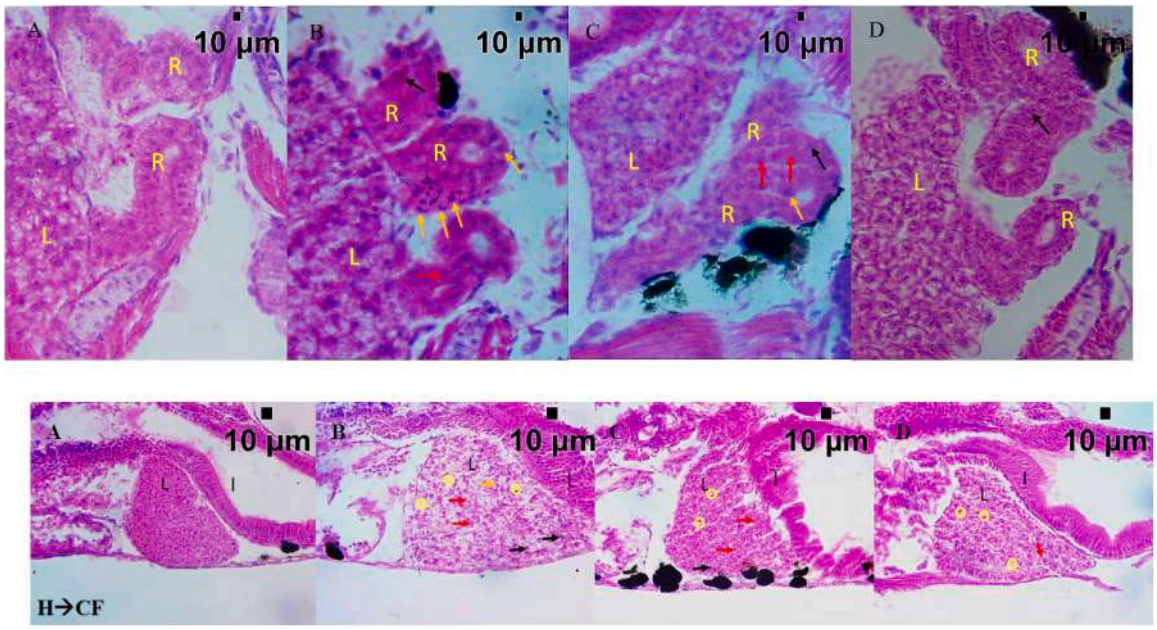

Fig. 9. Telomir-Zn reduces hepatorenal histopathological degeneration in ATP7Bˆ C271X zebrafish.
Representative hematoxylin and eosin (H&E)–stained cross-sections (400 × magnification) of zebrafish larvae. Top- Kidney tissue. Bottom – liver tissue. (A) Wild-type (Grade 0) showing normal hepatic architecture without evidence of vacuolization, necrosis, or inflammatory infiltration. (B) ATP7Bˆ C271X mutant (Grade 3) demonstrating severe degeneration characterized by extensive necrosis, cytoplasmic vacuolization, inflammatory cell infiltration, and structural disorganization. (C) Telomir-Zn 1.5 ng (Grade 2) showing partial preservation of hepatic architecture with reduced necrosis and inflammation. (D) Telomir-Zn 5 ng (Grade 1) demonstrating marked reduction in histopathological severity with minimal cellular swelling and limited inflammatory infiltration. Quantification of necrotic area and inflammatory infiltration is presented. Data are expressed as mean ± SEM. Statistical comparisons were performed as described in Methods.

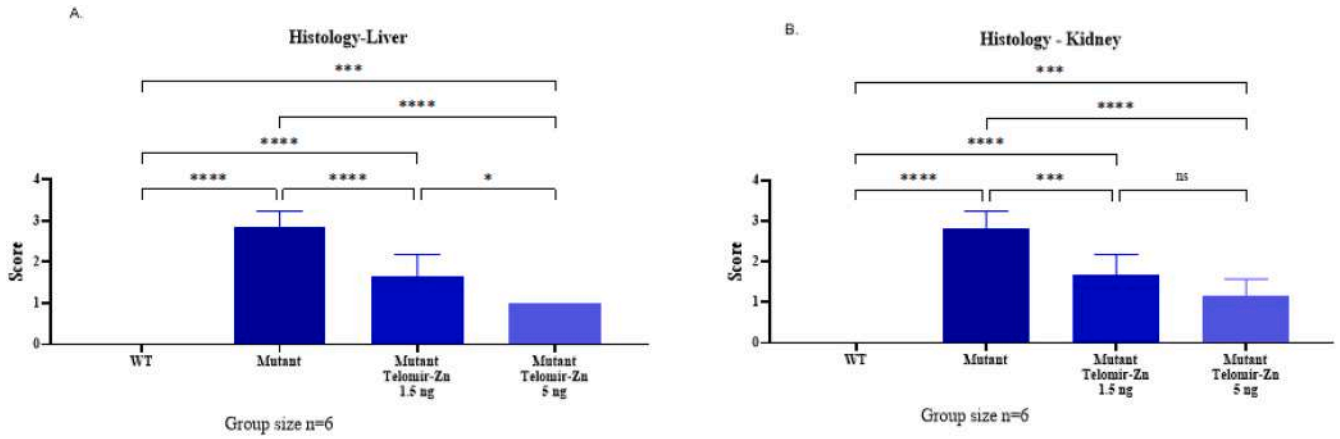

Fig. 10. Telomir-Zn reduces hepatic and renal copper burden in ATP7Bˆ C271X zebrafish.
(A) Histological scoring of hepatic copper-associated pathology. (B) Renal histological scoring. ATP7Bˆ C271X mutants exhibited elevated tissue copper accumulation relative to wild-type controls. Telomir-Zn treatment reduced hepatic and renal copper burden in a dose-dependent manner. Data are presented as mean ± SEM. Statistical comparisons were performed as described in Methods.

Importantly, the ~50% reduction in hepatic copper levels did not require complete copper normalization to achieve substantial phenotypic rescue, suggesting that attenuation of labile redox-active copper pools rather than total copper depletion may be sufficient to disrupt ROS–Ca^{2+} amplification cascades.

These findings highlight Telomir-Zn as a promising proof-of-concept agent for modulating intracellular metal redox balance and suggest that targeting labile copper pools may offer a complementary therapeutic strategy for Wilson's disease and other copper overload disorders

5. Conclusion

Modulation of labile copper pools attenuates copper-driven ROS amplification and intracellular Ca^{2+} dysregulation in human cell systems and is associated with improved functional and histological outcomes in ATP7B-deficient zebrafish. These findings support a model in which targeting redox-active copper disrupts ROS–Ca^{2+} feedback cascades and mitigates mitochondrial-associated tissue injury in copper overload.

Data availability

The datasets generated and analyzed during the current study are available from the corresponding author upon reasonable request.

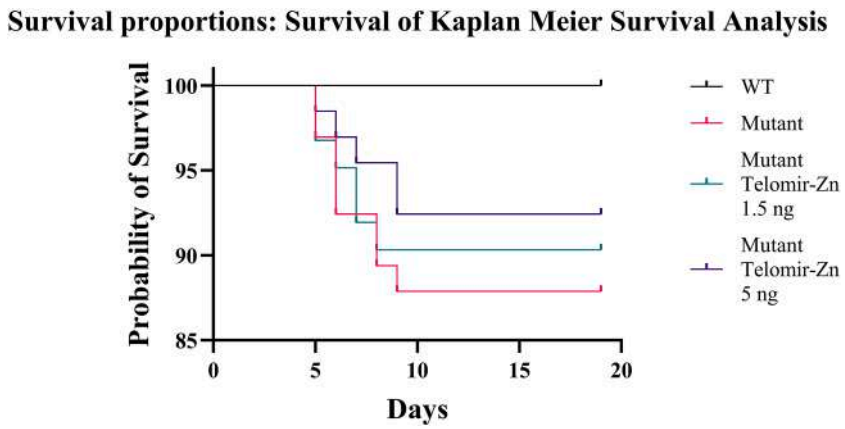

Fig. 11. Telomir-Zn improves survival in ATP7BˆC271X zebrafish.
Kaplan–Meier survival curves for wild-type, ATP7BˆC271X mutant, and Telomir-Zn–treated groups (1.5 ng and 5 ng). ATP7BˆC271X mutants exhibited reduced survival relative to wild-type controls. It is observed that, Mortality was absent in the wild-type (WT) group, indicating optimal survival under standard experimental conditions. In contrast, the ATP7B - C271X -/- mutant group showed a markedly increased mortality count of 12% of larvae, reflecting severe physiological compromise likely due to impaired metabolism and associated systemic toxicity. Treatment with Telomir-Zn demonstrated a dose-dependent reduction in mortality. At 1.5 ng, mortality decreased to 9% and further declined to 6% at the 5-ng dose.

Ethics statement

All animal procedures were conducted in accordance with institutional guidelines and approved by the appropriate animal care and use committees, in compliance with national regulations governing laboratory animal research. Ethical standards and principles of Good Animal Practice, as defined by the Institutional Animal Ethics Committee and in accordance with the guidelines of the Committee for the Control and Supervision of Experiments on Animals (CCSEA) in India and Association for Assessment and Accreditation of Laboratory Animal Care (AAALAC), were strictly followed.

Use of artificial intelligence

Artificial intelligence tools were used for language editing, formatting assistance, and production of graphical abstract. All scientific interpretation and conclusions were developed by the authors.

Funding

This work was supported by Telomir Pharmaceuticals Inc., which provided financial support for the conduct of the study.

CRediT authorship contribution statement

Itzchak Angel: Writing – review & editing, Writing – original draft, Validation, Supervision, Project administration, Methodology, Formal analysis, Conceptualization. **Kalaichitra Periyasamy:** Writing – review & editing, Supervision, Methodology. **Micha Gladnikoff:** Writing – review & editing, Methodology, Conceptualization. **Benin Joseph:** Writing – review & editing, Investigation, Conceptualization. **Raphael Mayer:** Writing – review & editing, Investigation, Conceptualization. **Erez Aminov:** Writing – review & editing, Writing – original draft, Funding acquisition, Conceptualization.

Declaration of competing interest

Erez Aminov is Chief Executive Officer of Telomir Pharmaceuticals Inc. Itzchak Angel is a consultant to Telomir Pharmaceuticals Inc. Some authors are affiliated with or receive compensation from Telomir Pharmaceuticals Inc. The remaining authors declare that they have no competing financial interests.

Acknowledgments

The authors thank the technical teams at Discovery Lab and Smart Assays Biotechnologies for their assistance with in vivo and in vitro experimental procedures.

References

[1] B. Halliwell, J.M.C. Gutteridge, Free Radicals in Biology and Medicine, 5th ed, Oxford University Press, 2015.
[2] M.C. Linder, Copper and genomic stability in mammals, Mutat. Res. 733 (1–2) (2012) 83–91.
[3] P. Tsvetkov, et al., Copper induces cell death by targeting lipoylated TCA cycle proteins, Science 375 (6586) (2022) 1254–1261, https://doi.org/10.1126/science.abf0529.
[4] E.A. Roberts, M.L. Schilsky, Diagnosis and treatment of Wilson disease: an update, Hepatology. 47 (6) (2008) 2089–2111, https://doi.org/10.1002/hep.22261.
[5] A. Członkowska, T. Litwin, P. Dusek, et al., Wilson disease, Nat. Rev. Dis. Primers 4 (2018) 21, https://doi.org/10.1038/s41572-018-0018-3.
[6] G.R. Martin, P. Tsvetkov, Fenton-like copper redox chemistry revisited: hydrogen peroxide and superoxide mediation of copper-catalyzed oxidant production, J. Inorg. Biochem. 125 (2013) 26–31, https://doi.org/10.1016/j.jinorgbio.2013.04.005.
[7] O. Bandmann, K.H. Weiss, S.G Kaler, Wilson's disease and other neurological copper disorders, Lancet Neurol. 14 (1) (2015) 103–113, https://doi.org/10.1016/S1474-4422(14)70190-5.
[8] L.M. Gaetke, C.K Chow, Copper toxicity, oxidative stress, and antioxidant nutrients, Toxicology 189 (1–2) (2003) 147–163, https://doi.org/10.1016/S0300-483X(03)00159-8.
[9] N. Keen, S. Lutsenko, Copper-induced translocation of the Wilson disease protein ATP7B: roles of COMMD1 and Rab7, Traffic 10 (2009) 379–391, https://doi.org/10.1111/j.1600-0854.2008.00875.x.
[10] S. Lutsenko, Human copper homeostasis mechanisms, J. Trace Elem. Med. Biol. 24 (2010) 146, https://doi.org/10.1016/j.jtemb.2010.02.001.
[11] H. Zischka, J. Lichtmannegger, Pathological mitochondrial copper overload in Wilson disease, Ann N Y Acad Sci. 1315 (2014) 6–15, https://doi.org/10.1111/nyas.1231.
[12] K.H. Weiss, et al., Bis-choline tetrathiomolybdate in patients with Wilson's disease: an open-label, multicentre, phase 2 study, Lancet Gastroenterol Hepatol. 2 (12) (2017) 869–876.
[13] J. Lichtmannegger, C. Leitzinger, R. Wimmer, S. Schmitt, S. Schulz, C. Eberhagen, et al., Methanobactin reverses acute liver failure in a rat model of Wilson disease, J. Clin. Invest. 126 (7) (2016) 2721–2735, https://doi.org/10.1172/JCI85226.
[14] R.S. Polishchuk, E.V. Polishchuk, From and to the Golgi: copper trafficking in health and disease, Biochim. Biophys. Acta Mol. Cell Res. 1865 (2018) 1914–1923, https://doi.org/10.1016/j.bbamcr.2018.10.005.
[15] J.M. Howell, J.K. Reed, Animal models of Wilson disease, J. Neurochem. 146 (2018) 356–373, https://doi.org/10.1111/jnc.14323.
[16] X. Chen, et al., Activation of HIF-1 signaling ameliorates liver steatosis through induction of pparγ-2 gene expression in liver-specific atp7b-deficient zebrafish, Toxicol. Appl. Pharmacol. 403 (2020) 115165, https://doi.org/10.1016/j.taap.2020.115165.
[17] S.R. Powell, The antioxidant properties of zinc, J. Nutr. 130 (2000) 1447S–1454S.

[18] W. Driever, L. Solnica-Krezel, A.F. Schier, S.C. Neuhauss, J. Malicki, D.L. Stemple, D.Y. Stainier, F. Zwartkruis, S. Abdelilah, Z. Rangini, J. Belak, C. Boggs, A genetic screen for mutations affecting embryogenesis in zebrafish, Development 123 (1996) 37–46.
[19] P.A. Cobine, D.C. Brady, Cuproptosis: cellular and molecular mechanisms underlying copper-induced cell death, Nat. Chem. Biol. 82 (2022) 1786–1787, https://doi.org/10.1016/j.molcel.2022.05.001.
[20] S. Du, G. Ma, X. Li, et al., Targeting ROS-metabolism dual pathways to trigger PANoptosis by cobalt-vanadium oxides biomimetic nanocakes for tumor immunotherapy, Biomaterials 326 (2026) 123726, https://doi.org/10.1016/j.biomaterials.2025.123726.
[21] Z. Wang, Y. Li, C. Wang, et al., Disrupting intracellular redox homeostasis through copper-driven dual cell death to induce anti-tumor immunotherapy, Biomaterials 324 (2026) 123523, https://doi.org/10.1016/j.biomaterials.2025.123523.
[22] D. Tang, X. Chen, R. Kang, G. Kroemer, Cuproptosis: molecular mechanisms and therapeutic implications, Cell Res. 32 (2022) 1047–1050.
[23] G.J. Brewer, Recognition, diagnosis, and management of Wilson's disease, Proc. Soc. Exp. Biol. Med. 223 (2000) 39–46.
[24] EASL Clinical Practice Guidelines: wilson's disease, J. Hepatol. 56 (2012) 671–685, https://doi.org/10.1016/j.jhep.2011.11.007.
[25] T.U. Hoogenraad, Paradigm shift in treatment of Wilson's disease: zinc therapy now treatment of choice, Brain Dev. 28 (3) (2006) 141–146.